Proceedings of the
47th IEEE Conference on Decision and Control
Cancun, Mexico, Dec. 9-11, 2008

Controlling Air and Burned Gas Masses of Turbocharged VVT SI Engines

Thomas Leroy, Jonathan Chauvin and Nicolas Petit

Abstract— **In this paper, we propose a strategy to control the in-cylinder air and burned gas masses inside the combustion chambers of turbocharged VVT SI engines. We coordinate existing low-level controllers acting separately on the throttle, the waste gate and on the VVT actuators. Coordination is obtained by updating the set points based on real-time measurements. The objective is to improve transients response. The effect of the implicit feedback loop is analyzed by the small-gain theorem.**

I. Introduction and motivations

The ever increasing European demands on fuel consumption and pollutant emissions reduction have lead to a sophistication of engine concepts and associated control technologies. Lately, downsizing (reduction of the engine size) has appeared as a major way to achieve those requirements for spark ignition (SI) engines. As was shown in [1] and [2], such downsized engines can reach high levels of performance and driveability, provided they are equipped with direct injection, turbocharger and Variable Valve Timing (VVT) actuators. Such a setup is represented in Figure 1. The cylinders are fed with fresh air from the throttle which is located downstream a compressor. The compressor is powered by the turbine located downstream the exhaust manifold. Indirectly, the waste gate controls the compression rate. VVT actuators impact on the timing of the intake and exhaust phases. Finally, combustion of the injected fuel takes place in the cylinders.

One essential task of engine control systems consists of managing the torque produced by the combustion according to the driver's requests. On SI engines, torque is controlled by managing the air mass aspirated into the cylinders, while keeping the Air/Fuel Ratio (AFR) close to the stoichiometric value to minimize exhaust (hydrocarbons, HC, nitrogen oxides, NO_x, and carbon monoxides, CO) emissions [3]. In turn, the in-cylinder air mass is controlled as follows. On conventional (fixed valve timing) engines, it is controlled by the throttle and the waste gate. By contrast, on variable valve timing engines, VVT actuators modify the in-cylinder composition by creating an Internal Exhaust Gas Recirculation (IEGR). Under partial engine load conditions, this permits to significantly increase the overall engine efficiency (mostly, by reducing pumping losses and NO_x emissions [4]). Under high engine load conditions, VVT actuators can be used to increase the air scavenging to improve the combustion efficiency [1].

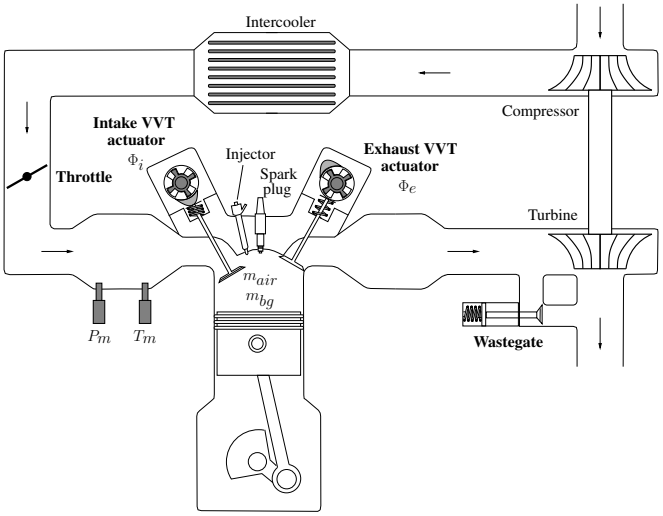

Fig. 1. Engine scheme. Intake manifold pressure and temperature, P_m and T_m, are measured by sensors. Φ_i and Φ_e are VVT actuators positions.

VVT actuators possess undebatable advantages in terms of combustion efficiency. However, analysis of the IEGR shows that it has some interaction with the slow intake manifold filling dynamics, which can cause unacceptable engine performance [5].

To compensate VVT actuators side effects, many authors have proposed transient control strategies. In [6], the authors present a dynamic camshaft scheduling based on throttle position and engine speed, to obtain a torque response similar to a fixed valve timing engine. Another point of view can be considered. In [7], [8] or [9], VVT actuators are seen as a disturbance for the in-cylinder air mass control. This disturbance is taken into account in the throttle control strategy. In these papers, valve timing devices are seen as a static function of the engine operating point. They are not used to reach any control objective.

In an attempt to move forward in the direction of combustion control, we propose to use the VVT actuators to control the in-cylinder burned gas mass. Compared to the previously mentioned studies, this represents an extra control objective. We control the in-cylinder gas masses (both air and burned gas), according to the VVT/intake manifold pressure model introduced in [10].

In details, we proceed as follows. Consider a turbocharged VVT SI engine, whose control system in-

T. Leroy (corresponding author) is a PhD Candidate in Mathematics and Control, Centre Automatique et Systèmes, École des Mines de Paris, 60, bd St Michel, 75272 Paris, France.
Email: *thomas.leroy@ensmp.fr*

J. Chauvin is with the Department of Engine Control in Institut Français du Pétrole, 1 et 4 Avenue de Bois Préau, 92852 Rueil Malmaison, France

N. Petit is with the Centre Automatique et Systèmes, École des Mines de Paris, 60, bd St Michel, 75272 Paris, France

cludes a low-level intake manifold pressure controller and a low-level VVT controller. Such controllers are exposed in [9], [8], [6], [11], [12], [13], [14]. In closed-loop, the intake manifold subsystem and the VVT subsystem have varying performance (mainly speed of convergence) over the whole engine conditions range. Their responses can be considered as moderately fast to slow, and, at occasions, they can outperform each other.

Our primary control objective is the in-cylinder air mass. Our secondary control objective is the in-cylinder burned gas mass. The strategy we propose aims at coordinating the two low-level control subsystems to improve the overall performance. When VVT actuators are slow, it is possible to adjust the intake manifold set point to speed-up the air feeding process. Conversely, under turbocharging conditions, one may wish to use the VVT to compensate the slow response of the intake manifold pressure due to the turbo-lag.

Preliminarily, we focus on atmospheric conditions. Explicitly, we compute set points for the two low-level controllers, based on real-time measurements of the intake manifold pressure and the VVT actuators positions. The induced feedback loop can be analyzed by the small-gain theorem.

The paper is organized as follows. In Section II, we present a model of the in-cylinder gas masses. Section III exposes the control strategy. We study the closed-loop behavior in Section IV. In Section V, we report experimental results. Finally, we conclude and give future directions in Section VI.

II. Modeling

A. Model definition

Consider the airpath of a turbocharged SI engine equipped with intake throttle, waste gate and dual independent VVT actuators as depicted in Figure 1. Notations are given in Table I.

TABLE I
NOMENCLATURE

Symbol	Description	Unit
ivc	Intake valve closing	deg
evc	Exhaust valve closing	deg
m_{air}	In-cylinder air mass	kg
m_{bg}	In-cylinder burned gas mass	kg
N_e	Number of crankshaft revolutions	rpm
OF	Overlap factor	$\mathrm{m}^2 \cdot \mathrm{deg}$
P_m	Intake manifold pressure	Pa
R	Ideal gas constant	J/kg/K
T_q	Torque	Nm
T_m	Intake manifold temperature	K
V_{ivc}	In-cylinder volume at ivc	m^3
V_{evc}	In-cylinder volume at evc	m^3
V_m	Intake manifold volume	m^3
Φ_i	Intake valve timing actuator position	deg
Φ_e	Exhaust valve timing actuator position	deg

To estimate the in-cylinder air and burned gas masses, we use the model presented in [10]

$$m_{bg} = \alpha_2 \frac{\mathrm{OF}}{N_e} + \alpha_3 V_{evc} \tag{1a}$$

$$m_{air} = \alpha_1 \frac{P_m}{RT_m} V_{ivc} - m_{bg} \tag{1b}$$

where α_1, α_2 and α_3 are known functions of P_m and N_e. V_{ivc} is the cylinder volume at intake valve closing (ivc). It is a function of intake valve timing, Φ_i. Similarly, V_{evc} is the cylinder volume at exhaust valve closing (evc). It is a function of exhaust valve timing, Φ_e. At last, the overlap factor (OF) [15] is a function of both intake and exhaust valve timings, Φ_i and Φ_e.

In-cylinder air mass model (1a)-(1b) has been identified on experimental engine test-bench measurements. By contrast with the in-cylinder air mass, experimentally burned gas rates are almost impossible to measure. However, a qualitative model (providing accurate estimates of the major trends) will appear sufficient for control purposes. The first term of the right-hand side of equation (1a) represents the burned gases flowing back to the intake pipe (back-flow phenomenon). It is a function of OF. The second term in the right-hand side stands for the amount of gases remaining in the cylinder from one cycle to the next. It is function of V_{evc}.

B. Model properties

Let $\Omega_{\Phi_i} = \left[\underline{\Phi}_i; \overline{\Phi}_i\right]$ be the set of feasible intake VVT actuator positions. Let $\Omega_{\Phi_e} = \left[\underline{\Phi}_e; \overline{\Phi}_e\right]$ be the set of feasible exhaust VVT actuator positions. Let Ω_p be the set of considered intake manifold pressure. Let Ω_{air} be the set of feasible air mass, and, finally, Ω_{bg} be the set of feasible burned gas mass.

We note $f : \Omega_p \times \Omega_{\Phi_i} \times \Omega_{\Phi_e} \to \Omega_{air}$ and $g : \Omega_p \times \Omega_{\Phi_i} \times \Omega_{\Phi_e} \to \Omega_{bg}$ such that

$$\begin{cases} m_{air} \triangleq f(P_m, \Phi_i, \Phi_e) \\ m_{bg} \triangleq g(P_m, \Phi_i, \Phi_e) \end{cases}$$

Due to the structure of α_1, α_2, α_3, OF, V_{ivc} and V_{evc} as functions of P_m, Φ_i, Φ_e, the three following partial inversibility assumptions hold (variables structures are given in [10]).

Assumption 1. *For all* $(\Phi_i, \Phi_e, m_{air}) \in \Omega_{\Phi_i} \times \Omega_{\Phi_e} \times \Omega_{air}$, *there exists a unique* $P_m \in \Omega_p$ *such that* $f(P_m, \Phi_i, \Phi_e) = m_{air}$.

Assumption 2. *For all* $(P_m, \Phi_e, m_{bg}) \in \Omega_p \times \Omega_{\Phi_e} \times \Omega_{bg}$, *there exists a unique* $\Phi_i \in \mathbb{R}$ *such that* $g(P_m, \Phi_i, \Phi_e) = m_{bg}$.

Assumption 3. *For all* $(P_m, \Phi_i, m_{bg}) \in \Omega_p \times \Omega_{\Phi_i} \times \Omega_{bg}$, *there exists a unique* $\Phi_e \in \mathbb{R}$ *such that* $g(P_m, \Phi_i, \Phi_e) = m_{bg}$.

From the above assumptions, (partial) inverse functions of f and g can be defined. We note $f^{-1}_{\Phi_i,\Phi_e} : \Omega_{air} \to \Omega_p$, $g^{-1}_{P_m,\Phi_e} : \Omega_{bg} \to \Omega_{\Phi_i}$ and $g^{-1}_{P_m,\Phi_i} : \Omega_{bg} \to \Omega_{\Phi_e}$, defined by the following relations for $(P_m, \Phi_i, \Phi_e) \in \Omega_p \times \Omega_{\Phi_i} \times \Omega_{\Phi_e}$

$$m_{air} = f(P_m = f^{-1}_{\Phi_i,\Phi_e}(m_{air}), \Phi_i, \Phi_e) \tag{2a}$$

$$m_{bg} = g(P_m, \Phi_i = g^{-1}_{P_m,\Phi_e}(m_{bg}), \Phi_e) \tag{2b}$$

$$m_{bg} = g(P_m, \Phi_i, \Phi_e = g^{-1}_{P_m,\Phi_i}(m_{bg})) \tag{2c}$$

In practice, VVT actuators can only admit bounded values. The inversion formula used in (2b) and (2c) may produce

infeasible values that need to be saturated before they can be used as input signals to the VVT control system. This point is addressed in the next section.

III. In-cylinder masses control strategy

Our control objective is to track set points for the in-cylinder air and burned gas masses. While the air-mass is an usual objective, because its value directly determines the produced torque, the in-cylinder burned gas mass has hardly been considered as a control objective before. Certainly, the in-cylinder burned gas mass is equivalent, *at steady-state*, to some VVT actuators positions. Yet, during transients, it seems unrelevant to give VVT actuators some precise positions based on *static* look-up tables which implicitly assume the system is at rest. Our point-of-view is that, during these transient phases, the actual control objective should be the in-cylinder burned gas mass, which directly impacts on the combustion, and on pollutant emissions.

A. Control scheme

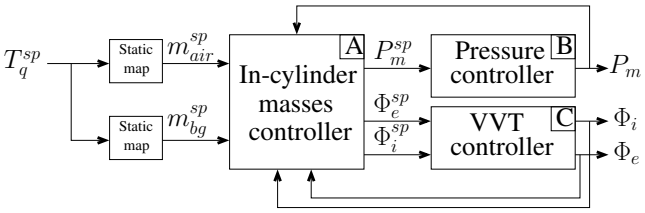

Fig. 2. Airpath control structure. Block A contains the contribution of the paper. Blocks B and C are the low-level pressure and VVT controllers.

Our contribution fits in the global airpath control scheme pictured in Figure 2. It is contained in block A which feeds two low-level controllers, the intake manifold pressure controller in block B and the VVT controller in block C. From T_q^{sp}, a torque requested by the driver through the accelerator pedal, static look-up tables are used to compute in-cylinder masses set points, m_{air}^{sp} and m_{bg}^{sp}. Physically, air and burned gas masses depend on the intake manifold pressure and the phasing of the distribution, i.e. the VVT actuators positions (see model (1a)-(1b)). Block A computes corresponding intake manifold pressure and VVT set points, P_m^{sp}, Φ_i^{sp} and Φ_e^{sp}. The closed-loops (from block B to A and from block C to A) feedback the current values of the intake manifold pressure and the VVT positions.

B. Controller design

We now give an explicit procedure to compute both intake manifold pressure and VVT actuators positions set points in order to reach the desired amounts of in-cylinder air and burned gases.

The in-cylinder masses set points, m_{air}^{sp} and m_{bg}^{sp}, are turned into physical variables set points on interest : an intake manifold pressure, P_m^{sp}, an intake VVT actuator position, Φ_i^{sp}, and an exhaust VVT actuator position, Φ_e^{sp}. To maximize the overall airpath control performance, in terms of in-cylinder masses tracking, a close-up analysis of the intake pressure and VVT low-level closed-loop response is necessary.

1) Intake pressure dynamics (block B): The intake manifold pressure satisfies a first order (slow filling) dynamics, derived from a balance equation in the intake manifold [3]. Under atmospheric conditions, although the pressure control is achieved thanks to the throttle which is fast, tracking of the pressure trajectory is limited by the boundedness of the air flow velocity. Under turbocharging conditions, even though the actuation structure changes (throttle is replaced by the waste gate), the intake pressure dynamics is limited by the turbocharger inertia. In summary, relatively slow responses must be expected from closed-loop controllers of the intake pressure dynamics (this point is supported in [11], [12]).

2) VVT dynamics (block C): Valve timings updates have an immediate effect on in-cylinder composition. These are obtained thanks to the VVT actuators which are electronically controlled hydraulic actuators. Their dynamics highly depend on internal oil pressure and temperature (see [13], [14]), which can affect the tracking of desired set points. These unknown disturbances slow-down the closed-loop response in a possibly unexpected way.

3) Control strategy: We propose to use the inverse model derived in Section II-B to compute set points for the low-level controllers. To account for the previously discussed slow responses of the corresponding subsystems, we coordinate them by replacing target set points by real-time measurements. Among the numerous possible solutions, we choose a technique which tries to satisfy both in-cylinder air mass and in-cylinder burned gas mass objectives.

Our primary control objective is the in-cylinder air mass because it directly impacts on the produced torque and the AFR. By comparison with intake manifold pressure, VVT actuators have limited effect on fresh air charge. Therefore, we use the intake manifold pressure as control variable for air mass control. From an in-cylinder air mass set point, we compute a pressure set point, P_m^{sp}, using equation (2a). In this formula, *we use VVT actuators positions measurements*. This gives

$$P_m^{sp} = f_{\Phi_i,\Phi_e}^{-1}(m_{air}^{sp}) \tag{3}$$

From (2a), it is obvious that (3) satisfies the primary control objective.

Our secondary control objective is the in-cylinder burned gas mass. The two remaining control variables are the VVT actuators. The burned gas system is over-actuated. First, we determine the intake valve timing, Φ_i, as a function ($h : \Omega_{air} \rightarrow \Omega_{\Phi_i}$) of the input m_{air}^{sp}. Look-up tables obtained for engine energetic optimization studies are used. Then, exhaust valve timing, Φ_e, remains as possible control variable for the burned gas mass control. Its set point Φ_e^{sp} is computed from in-cylinder burned gas mass set point. Again, to coordinate the two control subsystems and maximize speed of transient, *we substitute intake manifold pressure set point with measurements* (see (4a)). Finally, when the control variable Φ_e^{sp} becomes unfeasible (when exhaust VVT set point is out of the saturation bounds), it is saturated to the

maximum or minimum admissible value, and the left-over degree of freedom, Φ_i^{sp}, is used to minimize the induced burned gas mass mismatch (at the expense of the energetic efficiency). From (2b) and (2c), computation of the VVT positions set points writes

$$\Phi_e^{sp} = \psi_e\left(g^{-1}_{P_m,h(m_{air}^{sp})}(m_{bg}^{sp})\right) \tag{4a}$$

$$\Phi_i^{sp} = \begin{cases} h(m_{air}^{sp}) & \text{if } \Phi_e^{sp} \in \overset{\circ}{\Omega}_{\Phi_e} \\ \psi_i\left(g^{-1}_{P_m,\Phi_e^{sp}}(m_{bg}^{sp})\right) & \text{otherwise} \end{cases} \tag{4b}$$

where $\overset{\circ}{\Omega}_{\Phi_e}$ is the interior of Ω_{Φ_e}, ψ_i and ψ_e are saturation functions. $\psi_i(x) = x$ if $x \in \Omega_{\Phi_i}$, $\psi_i(x) = \underline{\Phi}_i$ when $x < \underline{\Phi}_i$ and $\psi_i(x) = \overline{\Phi}_i$ when $x > \overline{\Phi}_i$. $\psi_e(x) = x$ if $x \in \Omega_{\Phi_e}$, $\psi_e(x) = \underline{\Phi}_e$ when $x < \underline{\Phi}_e$ and $\psi_e(x) = \overline{\Phi}_e$ when $x > \overline{\Phi}_e$. From (2b) and (2c), it appears that, provided that at least one of the two VVT positions is not saturated, the observed in-cylinder burned gas mass reaches its set point.

The global control strategy is presented in Figure 3. Block A implements the high-level air and burned gas mass controller (3), (4a) and (4b).

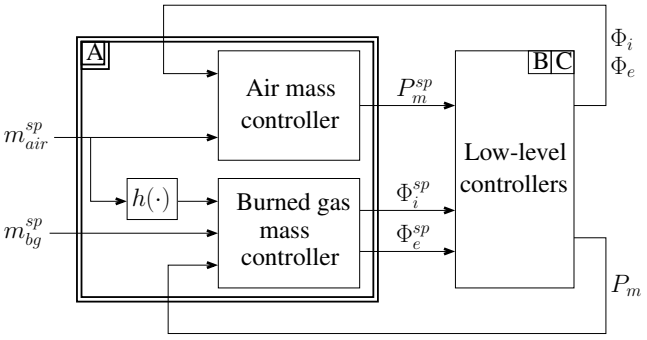

Fig. 3. Airpath Control strategy. Block A is the high-level air and burned gas mass controller, blocks B and C are the low-level pressure and VVT controllers.

IV. Stability proof

The previous section has introduced a high-level controller used at the input of both intake manifold pressure and VVT actuators controllers. To maximize performance, it uses real-time measurements in feedback loops. In general, the induced interconnection could cause trouble. As is now proven, this is not the case in unsaturated regimes (at first order). Analysis follows from the small-gain theorem. In the following, it is assumed that the intake manifold pressure and the VVT actuators satisfy some finite-gain $\mathcal{L}$ stable dynamics (with gains close to 1), similar to those observed in [9], [8], [6], [13], [14]. The controller static equations are linearized around a working point.

A. Linearization of the proposed controller

Consider the interconnection in Figure 3. Let $x \triangleq (P_m\ \Phi_i\ \Phi_e)^T$ be the states of blocks B and C and $u \triangleq (m_{air}^{sp}\ m_{bg}^{sp})^T$ be the input vector. Gathering equations (3), (4a) and (4b), the controller writes

$$\begin{cases} x_1^{sp} &= f^{-1}_{x_2,x_3}(u_1) \\ x_2^{sp} &= \begin{cases} h(u_1) & \text{if } x_3^{sp} \in \overset{\circ}{\Omega}_{\Phi_e} \\ \psi_i\left(g^{-1}_{x_1,x_3^{sp}}(u_2)\right) & \text{otherwise} \end{cases} \\ x_3^{sp} &= \psi_e\left(g^{-1}_{x_1,h(u_1)}(u_2)\right) \end{cases} \tag{5}$$

To simplify the stability analysis, we consider unsaturated conditions. Then, (5) becomes

$$\begin{cases} x_1^{sp} &= f^{-1}_{x_2,x_3}(u_1) \\ x_2^{sp} &= h(u_1) \\ x_3^{sp} &= g^{-1}_{x_1,h(u_1)}(u_2) \end{cases} \tag{6}$$

From (2a) and (2c), one can easily invert system (6). This yields

$$\begin{cases} u_1 &= f(x_1^{sp}, x_2, x_3) \\ u_2 &= g(x_1, h(u_1), x_3^{sp}) \end{cases} \tag{7}$$

Let $X^{\mathrm{o}} = (x_1^{\mathrm{o}}, x_2^{\mathrm{o}}, x_3^{\mathrm{o}}, u_1^{\mathrm{o}}, u_2^{\mathrm{o}}, x_1^{sp\mathrm{o}}, x_3^{sp\mathrm{o}})$ be a point in the neighborhood of $(x_1, x_2, x_3, u_1, u_2, x_1^{sp}, x_3^{sp})$. Linearization of (7) about X^{o} gives

$$\begin{cases} \delta u_1 = \left.\frac{\partial f}{\partial x_1}\right|_{X^{\mathrm{o}}} \delta x_1^{sp} + \left.\frac{\partial f}{\partial x_2}\right|_{X^{\mathrm{o}}} \delta x_2 + \left.\frac{\partial f}{\partial x_3}\right|_{X^{\mathrm{o}}} \delta x_3 \\ \delta u_2 = \left.\frac{\partial g}{\partial x_1}\right|_{X^{\mathrm{o}}} \delta x_1 + \left.\frac{\partial g}{\partial x_2}\right|_{X^{\mathrm{o}}} \left.\frac{\partial h}{\partial u_1}\right|_{X^{\mathrm{o}}} \delta u_1 + \left.\frac{\partial g}{\partial x_3}\right|_{X^{\mathrm{o}}} \delta x_3^{sp} \end{cases}$$

where

$$\begin{cases} \delta x_i &= x_i - x_i^{\mathrm{o}}, & \text{for } i = 1,2,3 \\ \delta x_i^{sp} &= x_i^{sp} - x_i^{sp\mathrm{o}}, & \text{for } i = 1,3 \\ \delta u_i &= u_i - u_i^{\mathrm{o}}, & \text{for } i = 1,2 \end{cases}$$

With vector notations $\delta x^{sp} \triangleq (\delta x_1^{sp}\ \delta x_2^{sp}\ \delta x_3^{sp})^T$, $\delta x \triangleq (\delta x_1\ \delta x_2\ \delta x_3)^T$ and $v \triangleq (v_1\ v_2\ v_3)^T$, one obtains

$$\delta x^{sp} = \begin{pmatrix} 0 & A_2 & A_3 \\ 0 & 0 & 0 \\ A_1 & 0 & 0 \end{pmatrix} \delta x + v \tag{8}$$

where

$$\begin{aligned} A_1 &= -\left.\frac{\partial g}{\partial x_3}\right|_{X^{\mathrm{o}}}^{-1} \cdot \left.\frac{\partial g}{\partial x_1}\right|_{X^{\mathrm{o}}}, \ A_2 = -\left.\frac{\partial f}{\partial x_1}\right|_{X^{\mathrm{o}}}^{-1} \cdot \left.\frac{\partial f}{\partial x_2}\right|_{X^{\mathrm{o}}}, \\ A_3 &= -\left.\frac{\partial f}{\partial x_1}\right|_{X^{\mathrm{o}}}^{-1} \cdot \left.\frac{\partial f}{\partial x_3}\right|_{X^{\mathrm{o}}} \end{aligned} \tag{9}$$

and

$$\begin{aligned} v_1 &= \left.\frac{\partial f}{\partial x_1}\right|_{X^{\mathrm{o}}}^{-1} \delta u_1, \ v_2 = \left.\frac{\partial h}{\partial u_1}\right|_{X^{\mathrm{o}}} \delta u_1, \\ v_3 &= \left.\frac{\partial g}{\partial x_3}\right|_{X^{\mathrm{o}}}^{-1} \left(\delta u_2 - \left.\frac{\partial g}{\partial x_2}\right|_{X^{\mathrm{o}}} \cdot \left.\frac{\partial h}{\partial u_1}\right|_{X^{\mathrm{o}}} \delta u_1\right) \end{aligned} \tag{10}$$

B. Stability analysis of the interconnection

Let $\mathcal{L}$ be the space defined as the set of all piecewise continuous functions $\varphi : [0, \infty[\to \mathbb{R}$ such that $\|\varphi\|_{\mathcal{L}} < \infty$, and $\mathcal{L}_e$ be its extended space (e.g. $\mathcal{L}$ can be any of the following spaces $\mathcal{L}_1$, $\mathcal{L}_2$, $\mathcal{L}_\infty$, see [16, p. 197]).

Consider the low-level intake manifold pressure and VVT controllers as nonlinear dynamical systems. Their linearized input-output relations are represented by

$$\delta x_i = H_i \delta x_i^{sp}, \text{ for } i = 1,2,3 \tag{11}$$

where $H_i : \mathcal{L}_e \rightarrow \mathcal{L}_e$. Figure 4 presents a schematic view of (8) and (11). In this figure, which in fact is equivalent to Figure 3 up to the change of variable (10), there are two interconnected systems: H_1 (the intake manifold pressure) and H_3 (the exhaust VVT actuator). Stability of the loop can be analyzed by the small-gain theorem. Note that H_2 does not influence the stability of the system (because we consider unsaturated regime (6)).

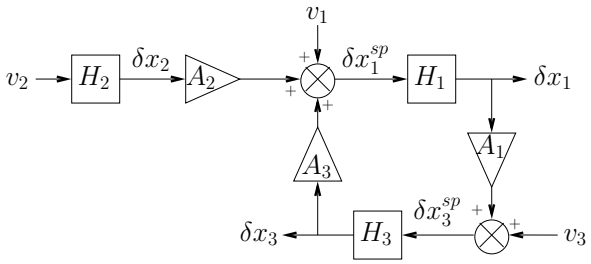

Fig. 4. Linearized control scheme. H_1, H_2 and H_3 are the systems of the low-level pressure and VVT controllers. H_1 and H_3 are interconnected systems.

Suppose that both systems H_1 and H_3 are finite-gain $\mathcal{L}$ stables (i.e. both low controllers are well behaved), that is

$$\begin{aligned}\|\delta x_{1\tau}\|_{\mathcal{L}} &\leq \gamma_1 \|\delta x_{1\tau}^{sp}\|_{\mathcal{L}} + \beta_1, \ \forall \delta x_1^{sp} \in \mathcal{L}_e, \ \forall \tau \in [0, \infty[\\ \|\delta x_{3\tau}\|_{\mathcal{L}} &\leq \gamma_3 \|\delta x_{3\tau}^{sp}\|_{\mathcal{L}} + \beta_3, \ \forall \delta x_3^{sp} \in \mathcal{L}_e, \ \forall \tau \in [0, \infty[\end{aligned}$$

where γ_1, γ_3, β_1 and β_3 are nonnegative constants and, for all signal u, u_τ is the truncation of u over $[0; \tau]$. Now, from the small-gain theorem (see [16, theorem 5.6]), the following proposition holds

Proposition 1. *The feedback connection is finite-gain $\mathcal{L}$ stable if $\gamma_1\gamma_3 \|A_1\|_{\mathcal{L}} \|A_3\|_{\mathcal{L}} < 1$.*

Consider well-behaved intake manifold pressure and VVT controllers, with $\mathcal{L}$ gains close to 1, say such that

$$\gamma_1\gamma_3 \ < \ 1 + \gamma$$

Usually, $\beta_1 = 0$ and $\beta_3 = 0$ under the assumption of zero-bias closed-loop response.

From (9), the product $\|A_1\|_{\mathcal{L}} \|A_3\|_{\mathcal{L}}$ writes

$$\|A_1\|_{\mathcal{L}} \|A_3\|_{\mathcal{L}} = \left\| \left.\frac{\partial g}{\partial x_3}\right|_{X^o}^{-1} \cdot \left.\frac{\partial g}{\partial x_1}\right|_{X^o} \cdot \left.\frac{\partial f}{\partial x_1}\right|_{X^o}^{-1} \cdot \left.\frac{\partial f}{\partial x_3}\right|_{X^o} \right\|_{\mathcal{L}} \tag{12}$$

From (1b), it comes

$$\left.\frac{\partial f}{\partial x_3}\right|_{X^o} = - \left.\frac{\partial g}{\partial x_3}\right|_{X^o} \tag{13}$$

Gathering (12) and (13), yields

$$\|A_1\|_{\mathcal{L}} \|A_3\|_{\mathcal{L}} = \left\| \left.\frac{\partial g}{\partial x_1}\right|_{X^o} \cdot \left.\frac{\partial f}{\partial x_1}\right|_{X^o}^{-1} \right\|_{\mathcal{L}}$$

Interestingly, this product remains strictly below 1 over the whole range of operating points under consideration for turbocharged VVT SI engines. Indeed, Figure 5 reports the value of $\|A_1\|_{\mathcal{L}} \|A_3\|_{\mathcal{L}}$ for different engine torque and speed. A physical interpretation is that the in-cylinder air mass has a higher intake manifold pressure dependency than the in-cylinder burned gas mass.

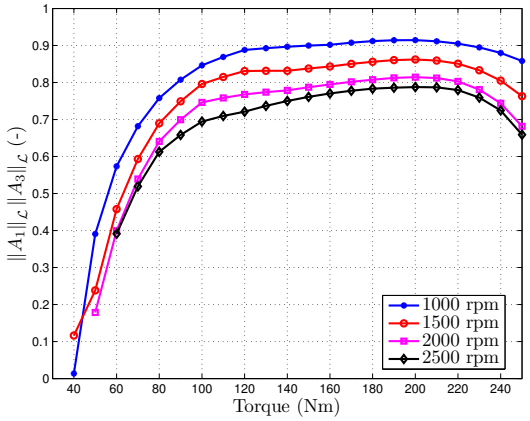

Fig. 5. Product $\|A_1\|_{\mathcal{L}} \|A_3\|_{\mathcal{L}}$ as a function of torque and engine speed.

In summary, provided that γ is sufficiently small (which is reasonably expected from the low-level controllers), Proposition 1 holds.

V. Experimental results

The proposed control strategy (5) has been embedded into a real-time control target and tested at test-bench.

A. Experimental setup

The engine under consideration is a 1,8L four-cylinder SI engine using direct injection and homogeneous combustion [17]. The airpath consists of a turbocharger controlled by a waste-gate, an intake throttle and a downstream-compressor heat exchanger permitting intake air temperature regulation. To take advantage of all the versatility of direct injection and turbocharging, the engine is equipped with two variable valve timing devices, for intake and exhaust valves. This engine setup is consistent with the scheme reported in Figure 1.

B. Burned gas mass variations

The first scenario under consideration consists of requesting various burned gas mass set points for a constant air mass set point. This scenario is of particular interest during test-bench engine energetic optimization process, when for a given torque set point, the optimal in-cylinder burned gas mass is sought with respect to minimum pollutant emissions criteria.

Figure 6a represents the in-cylinder burned gas mass set point, m_{bg}^{sp}, and its estimation given by model (1a), m_{bg}. Although the model cannot be compared with any measurement, NO_x measurements in Figure 6e shows the consistency of the in-cylinder burned gas model (increase of the burned gas fraction decreases NO_x emissions, see [3]). Figure 6b gives the in-cylinder air mass set point (constant), m_{air}^{sp}, its measurement, m_{air}^{meas}, given by the air flow sensor, and its estimation (1b), m_{air}. It reveals a good fit between the in-cylinder air mass model and measurements.

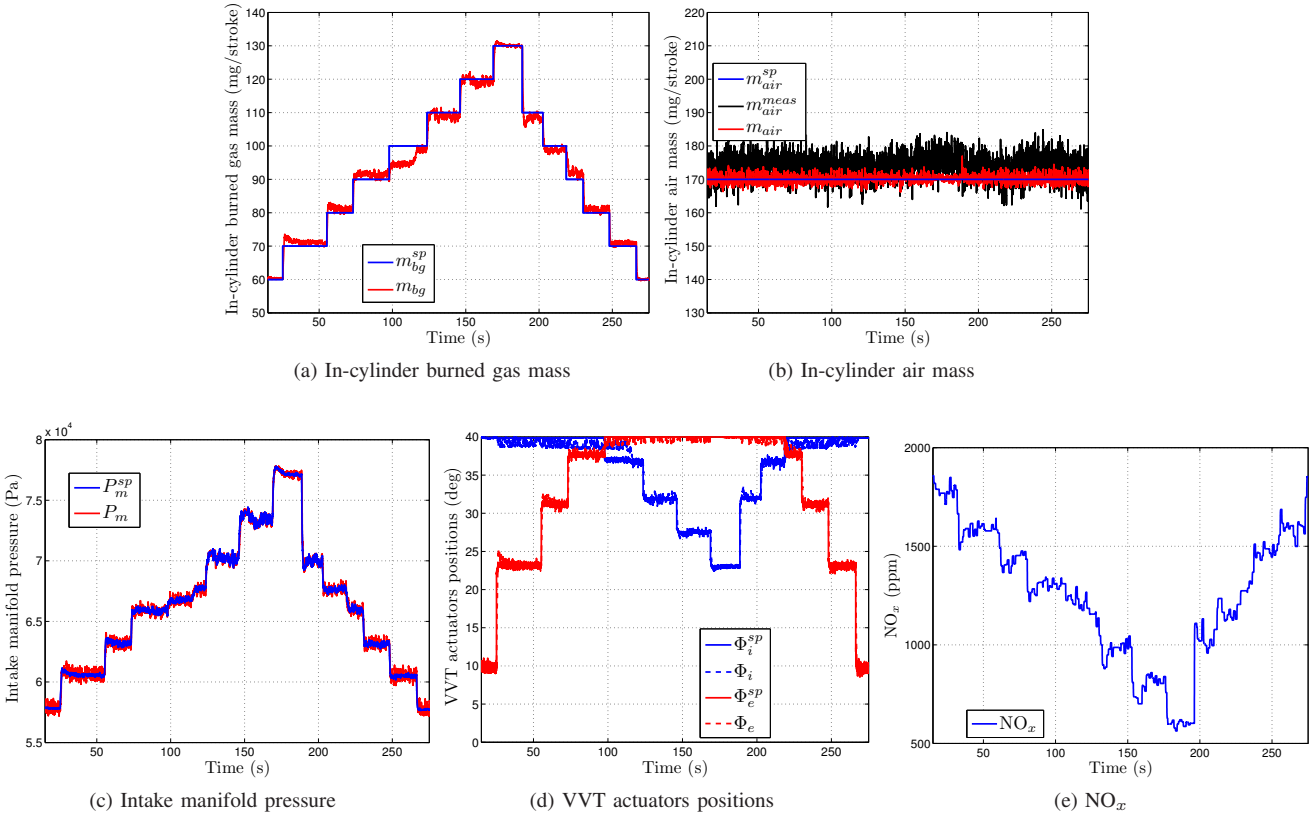

(a) In-cylinder burned gas mass (b) In-cylinder air mass

(c) Intake manifold pressure (d) VVT actuators positions (e) NO_x

Fig. 6. Experimental results on a 4-cylinder turbocharged VVT SI engine at constant engine speed (2000 rpm). Variation of in-cylinder burned gas mass at constant in-cylinder air mass.

The proposed controller succeeds in fulfilling both objectives by manipulating simultaneously the intake manifold pressure and the VVT actuators. It is worth noticing that the limitations of the VVT actuators positions values are fully accounted for. This point is particularly visible over the time interval $100 - 220$ s, in Figure 6d, when the exhaust VVT actuator saturates to its maximum value while the intake VVT is automatically used to compensate the possibly induced mismatch of the in-cylinder burned gas mass. As a result, the in-cylinder burned gas mass perfectly tracks its reference, except right after $t = 100$ s. Interestingly, the response at time 100 s shows how the proposed controller uses the intake manifold pressure set point as a degree of freedom to compensate the temporary "sticking" of the intake VVT actuator (see Figure 6c). Thanks to this insightful decision, the in-cylinder air mass remains at its set point.

C. Torque transients

The transient response observed in Figure 7 is particularly interesting. In this scenario, a torque transient is requested by the driver. This defines an increase in the in-cylinder air mass set point. Similarly, the set point of burned gas mass increases too. To perform this transient, both the intake manifold pressure and the VVT actuators must be controlled. Our proposed controller coordinates both the pressure and the VVT controllers. The VVT actuators behave relatively poorly (see Figure 7d), which is detected by the controller. To account for the discrepancy between the exhaust VVT set point and its actual position, the intake manifold pressure set point features a sharp change of slope in the middle of the transient (see Figure 7c). This avoids a possible overshoot in the observed in-cylinder air mass (see Figure 7b; overshoot and undershoot of the measurements are due to the sensor location - upstream the compressor -, it does not capture the intake filling dynamics). The primary control objective is fulfilled. The air mass transient is fast and accurate. Besides, the burned gas mass smoothly reaches its set point at its own speed as the VVT actuators eventually converge (see Figure 7a). A similar, but slightly less visible, behavior takes place at the following tip-out.

VI. Conclusion and Future Direction

The paper presents a control strategy to manage both the in-cylinder air and burned gas masses on engines equipped with VVT actuators. The method consists of computing intake manifold pressure and VVT actuators set points to coordinate the low-level controllers. It uses real-time measurements in feedback loops. Stability of the created interconnected closed-loop system is analyzed through the small gain theorem. Experimental results obtained at test-bench stress the relevance of the control strategy.

The strategy has been validated under atmospheric conditions. We plan to test the control strategy on the whole engine operating area.

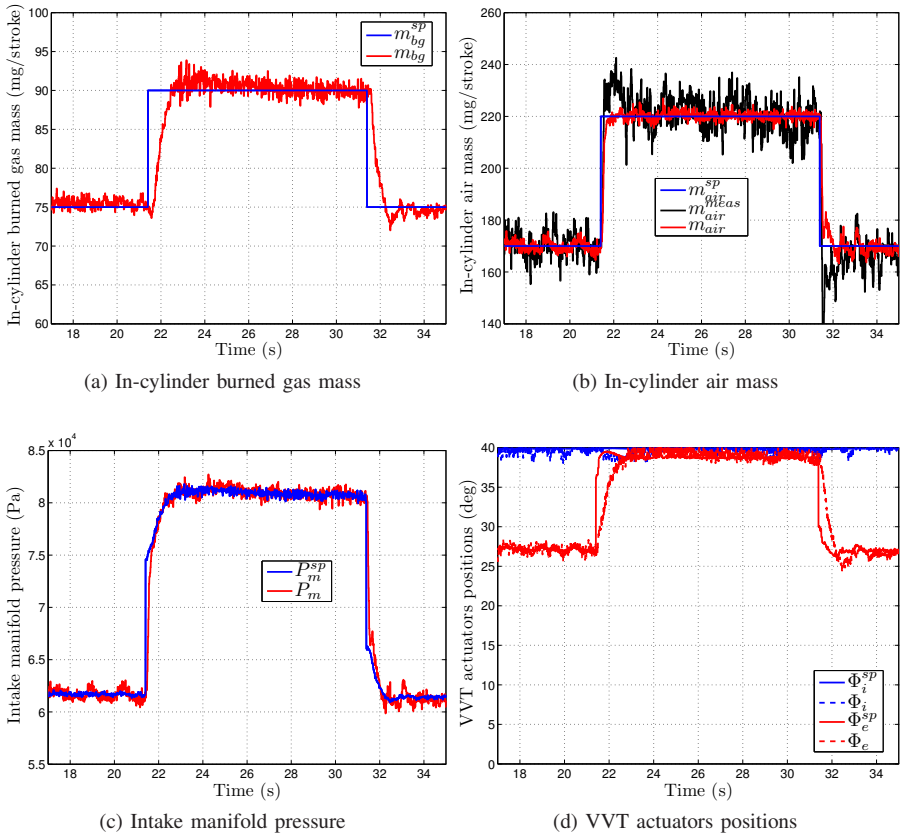

(a) In-cylinder burned gas mass (b) In-cylinder air mass

(c) Intake manifold pressure (d) VVT actuators positions

Fig. 7. Experimental torque transients on a 4-cylinder turbocharged VVT SI engine at constant engine speed (2000 rpm).

ACKNOWLEDGMENTS

The authors would like to gratefully thank Gilles Corde for his scientific support.

REFERENCES

[1] B. Lecointe and G. Monnier, "Downsizing a gasoline engine using turbocharging with direct injection," in *Proc. of SAE Conference*, no. 2003-01-0542, 2003.

[2] H. Kleeberg, D. Tomazic, O. Lang, and K. Habermann, "Future potential and development methods for high output turbocharged direct injected gasoline engines," in *Proc. of SAE Conference*, no. 2006-01-0046, 2006.

[3] J. Heywood, *Internal Combustion Engine Fundamentals*. McGraw-Hill, Inc, 1988.

[4] T. Leone, E. Christenson, and R. Stein, "Comparison of variable camshaft timing strategies at part load," in *Proc. of SAE Conference*, no. 960584, 1996.

[5] A. Stefanopoulou and I. Kolmanovsky, "Analysis and control of transient torque response in engines with internal exhast gas recirculation," in *IEEE Transactions on Control Systems Technology*, vol. 7, no. 5, 1999, pp. 555–566.

[6] ——, "Dynamic scheduling of internal exhaust gas recirculation systems," in *Proc. IMECE*, vol. 61, 1997, pp. 671–678.

[7] M. Jankovic, F. Frischmuth, A. Stefanopoulou, and J. Cook, "Torque management of engines with variable cam timing," in *Control Systems Magazine, IEEE*, vol. 18, 1998, pp. 34–42.

[8] M. Jankovic, "Nonlinear control in automotive engine applications," in *in Proc. of 15th International Symposium on Mathematical Theory of Networks and Systems*, 2002.

[9] T. Leroy, J. Chauvin, and N. Petit, "Airpath control of a SI engine with variable valve timing actuators," in *Proc. of the American Control Conference*, 2008, to appear.

[10] T. Leroy, J. Chauvin, F. Le Berr, A. Duparchy, and G. Alix, "Modeling fresh air charge and residual gas fraction on a dual independant variable valve timing SI engine," in *Proc. of SAE Conference*, no. 2008-01-0983, 2008.

[11] A. Stefanopoulou, I. Kolmanovsky, and J. Freudenberg, "Control of variable geometry turbocharged diesel engines for reduced emissions," in *IEEE Transactions on Control Systems Technology*, vol. 8, no. 4, 2000, pp. 733 – 745.

[12] D. Schwarzmann, R. Nitsche, and J. Lunze, "Diesel boost pressure control using flatness-based internal model control," in *Proc. of SAE Conference*, no. 2006-01-0855, 2006.

[13] J. Chauvin and N. Petit, "Experimental control of variable cam timing actuators," in *Proc. of IFAC Automotive Control*, 2007.

[14] A. Genç, K. Glover, and R. Ford, "Nonlinear control of hydraulic actuators in variable cam timing engines," in *International IFAC Workshop on Modeling, Emissions and Control in Automotive Engines*, 2001.

[15] J. Fox, W. Cheng, and J. Heywood, "A model for predicting residual gas fraction in spark-ignition engines," in *Proc. of SAE Conference*, no. 931025, 1993.

[16] H. Khalil, *Nonlinear Systems*. Prentice-Hall, Inc., 1992.

[17] G. Le Solliec, F. Le Berr, G. Colin, G. Corde, and Y. Chamaillard, "Engine control of a downsized spark ignited engine: from simulation to vehicle." in *Proc. of ECOSM Conference*, 2006, pp. 153–168.